Research Article

A Graphical Robust PID Controller Design for Time-Varying Uncertain Systems with Applications to Trajectory Tracking of a Load-Varying Rigid SCARA

Pinit Ngamsom*
Department of Mechanical Engineering, College of Engineering,
Rangsit University, Phaholyothin Road, Lak-Hok, Pathum Thani 12000, Thailand

Abstract

We proposed in this paper a robust graphical PID controller design technique for trajectory tracking of rigid SCARAs carrying loads with time-varying mass and mass moment of inertia. Because of the time-varying loads and coupled nonlinearities in error dynamics of the tracking control system, the system matrix and the input matrix of the corresponding linearized model about the equilibrium point at the origin were time-varying. Existing robust PID controller design techniques formulated without handling this difficulty were then theoretically lacking. Our controller design technique yielded a 3D graph that could be employed to generate a PID control law that guaranteed input-to-state stability of the resulting control system by using the Lyapunov stability theorem. Simulation results were provided to confirm this. We compared our results with those obtained from using an existing sliding-mode control technique, and constructively drew out relevant characteristics that could be useful for the application of interest.

Keywords: manipulator; robot; stability; robustness; tracking; PID; loading variation

1. Introduction

Applications of robots are now common for many types of industries because they can offer several distinct advantages over conventionally dedicated machines. One of these is the flexibility of their trajectory tracking capability, which may be employed for a large variety of tasks such as arc welding in the metal manufacturing industry and paint spraying in the automotive industry. Controller design for trajectory tracking of a robot with multiple revolute joints is theoretically challenging because, in general, the robot in itself is a strongly coupled nonlinear system. On top of this, trajectory tracking adds coupled time-varying characteristics to the system. Despite of these difficulties, linear PID controllers are widely adopted for robotic applications in many industries because of their simplicity, availability, and satisfactory results they could produce [1]. Linear models used in a large number of existing robust PID controller design techniques may be obtained by

***Correspondence** : ngamsomp@hotmail.com

DOI 10.14456/tijsat.2016.12

linearizing the corresponding nonlinear model about an operating point [2], by neglecting nonlinear coupled dynamics of the robot and considering only linear dynamics of the joint actuators [3], or by computing torque to cancel out nonlinear terms in the equation of motion [4]. Usually, all the uncertain parameters associated with these linear models are assumed to be constants. Then, the controllers may be obtained simultaneously for all joints, or independently for each joint. Stability and tracking performance are usually investigated by doing numerical simulations. In practices, successes of these approaches are widely recognized by the industry for set point regulation. For trajectory tracking of a robot with multiple revolute joints, such linear models could not accurately represent dynamics of the system even in small neighborhoods about the operating point of interest. Accordingly, stability and performance of the resulting PID controllers could be inconsistent when trajectories change significantly. Theoretically, this is not surprising given that the robot trajectory control system is indeed a highly coupled nonlinear time-varying system operating in a generally large workspace. New sets of parameters are usually needed for the PID controllers to achieve satisfactory level of performance in this situation. However, it usually takes considerable time to find a set of controller parameters that yields satisfactory tracking performance [1].

For robotic trajectory tracking, a variety of sliding-mode control techniques have been explored in many researches. This is primarily because the associated principle allows strong robustness for the resulting control systems [5-10]. However, for robotic systems with multiple revolute joints, the associated control laws usually comprise of multiple complicated switching terms. It is well known that these terms could produce chattering on control input and excite hidden dynamics. Also, it could appear in typical experiments that these are associated with considerable amount of heat in amplifiers. Subsequently, various improvements and partial solutions to these undesirable characteristics have been reported [5, 9-10, 12-13]. Yet, it is not always clear when we could expect tracking performance enhancement from these complex techniques. Indeed, joint tracking errors resulting from a PID control system could be smaller than those from sliding-mode control systems in certain situations [1].

In contrast to existing robust PID controller design techniques discussed previously, ours allows consistency of stability and performance for trajectory tracking in large workspaces. This starts by not neglecting relevant time-varying terms after linearization so that our model represents the tracking dynamics in small neighborhoods about the operating point of interest better than a linear model with all constant parameters does. Our linear state feedback control law could also be favorable to existing switching control laws because it is smooth, is relatively simple to obtain, and is easy to implement.

This paper examines in Section 2 the situation in which a nonlinear model of a rigid SCARA (Selective Compliance Assembly Robot Arm) is set for trajectory tracking using joint errors and joint velocities as feedback states. When the resulting model is linearized about the equilibrium point at the origin, time-varying terms appear in both the system matrix and the input matrix. These terms appear because of the time-varying nature of reference trajectories and loading variations. Their magnitudes could be large even in small neighborhoods about the origin, and thus they should not be neglected if modeling accuracy is required. Accordingly, we admit this linear time-varying model for our PID controller design. Our controller design is a graphical approach. We develop in Section 3, a 3D graph of a particular real computational result versus two real controller design parameters. A stabilizing controller is found when the graph is negative at some point. Stability of the resulting tracking control system is then theoretically guaranteed. Section 4 contains a numerical example in which we verify stability and examine tracking performance of the resulting control system. These results are compared with those from a sliding-mode control approach. From this, desirable properties of our PID controller are finally evident. The paper is concluded in Section 5.

2. Mathematical Models

Important dimensions and variables of a typical SCARA carrying a loading object are shown in Figure 1. The corresponding dynamics is well known, and we present here for convenience of the readers a mathematical model of a typical SCARA operating in the horizontal plane XY:

$$M\ddot{q} + C = T_c + T_d \tag{1}$$

where the vectors $q = [q_1 \quad q_2]^T$, $T_c = [T_{c1} \quad T_{c2}]^T$, and $T_d = [T_{d1} \quad T_{d2}]^T$ are joint angle, control torque, and external disturbing torque respectively.

Although robot dynamics in Eq. (1) is well understood, we provide here for convenience of the readers all the elements of $M \in \Re^{2\times2}$ and $C \in \Re^{2\times1}$:

$$\begin{aligned} M_{11} = {} & m_1L_{c1}^2 + m_2(L_1^2 + L_{c2}^2) + m_p(L_1^2 + L_2^2) \\ & +2L_1(m_2L_{c2} + m_pL_2)\cos(q_2) + I_1 + I_2 + I_p, \end{aligned}$$

$$\begin{aligned} M_{12} = {} & m_2L_{c2}^2 + m_pL_2^2 + I_2 + I_p \\ & + L_1(m_2L_{c2} + m_pL_2)\cos(q_2) = M_{21}, \end{aligned}$$

$$M_{22} = m_2L_{c2}^2 + m_pL_2^2 + I_2 + I_p,$$

$$C_1 = -L_1(m_2L_{c2} + m_pL_2)(2\dot{q}_1\dot{q}_2 + \dot{q}_2^2)\sin(q_2),$$

$$C_2 = L_1(m_2L_{c2} + m_pL_2)\dot{q}_1^2\sin(q_2)$$

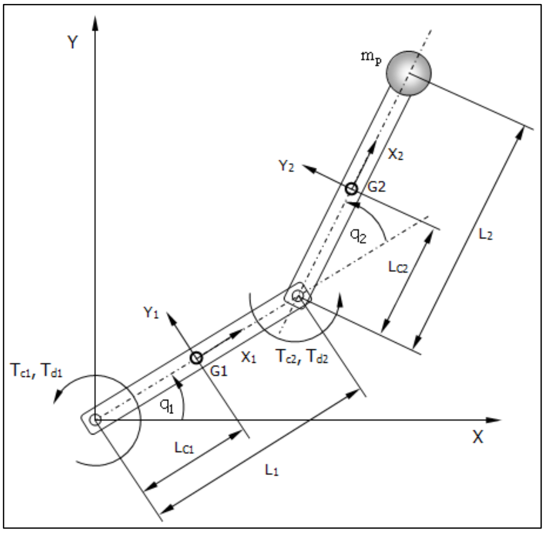

Figure 1. Typical Dimensions of a SCARA with Loading Object $m_p(t)$.

Note that m_i and I_i, i = 1, and 2 are mass and polar mass moment of inertia of link i respectively. It was shown in [12] that robot parameters could be determined very accurately and the computed torque technique could yield satisfactory tracking performance. With advances in measurement and computational techniques available now, it is then reasonable to expect that relevant robot parameters could be determined very accurately. Accordingly, the controller need not be very robust to these parameter uncertainties. However, it is unavoidable in many practices that the robot is to carry a relatively large tool or loading object of time-varying mass and mass moment of inertia. We then consider in this paper the case in which the tip of link 2 is attached with a loading object of time-varying mass $m_p(t)$ and polar mass moment of inertia $I_p(t)$. It can be shown that we can write $I_p = c_pm_p$ where $c_p \in \Re^+$ depends on the shape of the object. For a homogeneous cylinder of mass m_p and radius r_p, we have $I_p = (1/2)m_pr_p^2$ and $c_p = (1/2)r_p^2$. Without loss of generality, we assume that the shape of the object is fixed and

c_p is a constant because the time-varying case for c_p may be handled in the same fashion as we do for m_p.

To facilitate our analysis, we rewrite Eq. (1) to obtain:

$$\ddot{q}_1 = -\frac{\begin{pmatrix} 2a_2a_3\sin(q_2)(\dot{q}_1+\dot{q}_2)^2 \\ +a_3^2\dot{q}_1^2\sin(2q_2)+2a_2(T_{c1}+T_{d1}) \\ -2(a_2+a_3\cos(q_2))(T_{c2}+T_{d2}) \end{pmatrix}}{a_3^2(1+\cos(2q_2))-2a_1a_2}$$

$$\ddot{q}_2 = \frac{\begin{pmatrix} 2a_2a_3\sin(q_2)(\dot{q}_1+\dot{q}_2)^2 \\ +a_3^2\sin(2q_2)(2\dot{q}_1^2+2\dot{q}_1\dot{q}_2+\dot{q}_2^2) \\ +2a_1a_3\sin(q_2)\dot{q}_1^2 \\ +2(a_2+a_3\cos(q_2))(T_{c1}+T_{d1}) \\ -2(a_1+a_2+2a_3\cos(q_2))(T_{c2}+T_{d2}) \end{pmatrix}}{a_3^2(1+\cos(2q_2))-2a_1a_2}$$

where parameters a_i, i = 1, 2, and 3 depend on link lengths and mass properties of the robot as:

$$a_1 = m_1L_{c1}^2+(m_2+m_p)L_1^2+I_1,$$

$$a_2 = m_2L_{c2}^2+m_pL_2^2+I_2+I_p,$$

$$a_3 = L_1(m_2L_{c2}+m_pL_2)$$

We now define joint error variables $e_i = r_i - q_i$, where r_i is the joint reference signal. Then substitute $q_i = r_i - e_i$ and the corresponding first two derivatives in the above two equations to obtain tracking error dynamics of the robot in vector-matrix form:

$$\ddot{e} = f(e_i,\dot{e}_i,r_i,\dot{r}_i,\ddot{r}_i,m_p)+g(e_i,r_i,m_p)(T_c+T_d) \quad (2)$$

where $e = [e_1 \quad e_2]^T$, and $f = [f_1 \quad f_2]^T$ are the error vector and a nonlinear vector, respectively. It can be shown that the origin is an equilibrium point of Eq. (2) when all the torques and derivatives of all the joint reference signals are zero. A linear approximation of Eq. (2) about the origin is given by:

$$\begin{aligned}\ddot{e}_i &= \sum_{j=1}^{2}\left(\frac{\partial f_i}{\partial e_j}e_j+\frac{\partial f_i}{\partial \dot{e}_j}\dot{e}_j\right) \\ &\quad +\sum_{j=1}^{2}\bar{g}_{ij}T_{cj}+\bar{f}_i+\sum_{j=1}^{2}\bar{g}_{ij}T_{dj}\end{aligned} \quad (3)$$

where i = 1 and 2, j = 1 and 2, and all the partial derivatives, $\bar{f}_i$, and $\bar{g}_{ij}$ are evaluated at the origin. Note that Eq. (3) is a valid approximation of Eq. (2) when the control torques are capable of containing the trajectory of interest in small neighborhoods about the origin. In set point regulation problems, r_i is a constant and all derivatives of r_i with respect to time are then zero. It follows that all the partial derivatives, $\bar{f}_i$, and $\bar{g}_{ij}$ in Eq. (3) are constants, and thus the problem of stabilizing Eq. (3) is significantly simplified. When r_i is a function of time as in trajectory tracking problems, these terms are also functions of time. Accordingly, Eq. (3) is a time-varying system. In this paper, it is the problem of stabilizing this time-varying system for which we propose our controller.

We now define six state variables for our PID control system as $x_1 \equiv \int e_1 dt$, $x_2 \equiv \int e_2 dt$, $x_3 \equiv e_1$, $x_4 \equiv e_2$, $x_5 \equiv \dot{e}_1$, and $x_6 \equiv \dot{e}_2$. Combining these definitions with Eq. (3), we can write the model:

$$\dot{x} = [A+\Delta A(t)]x+[B+\Delta B(t)]u+w(t) \quad (4)$$

where $x \in \Re^n$ with n = 6 is the state vector, the system matrix $A \in \Re^{n\times n}$ is known, the input matrix $B \in \Re^{n\times m}$ with m = 2 is known, $u \equiv [T_{c1} \quad T_{c2}]^T$ is the control input vector, and the bounded time-varying perturbation vector $w(t) \in \Re^n$ contains all $\bar{f}_i$ and $\bar{g}_{ij}T_{dj}$. The symbol Δ denotes time-varying matrices resulting from the time-varying reference signals. For the SCARA of interest, time-varying elements of ΔA are (5, 4), (5, 5), (5, 6), (6, 4), (6, 5), and (6, 6), while those of ΔB are (5, 1), (5, 2), (6, 1), and (6, 2). Totally, we have N = 10 time-varying elements. All of them are associated with known upper and lower bounds that depend on the joint reference signals and their first two time derivatives. The control inputs vector, the perturbation vector, and all the time-varying elements are assumed to be uniformly globally Lipschitz.

3. Controller Design

Our PID controller employs the linear state-feedback control law $u = -Kx$, where $K \in \Re^{m\times n}$ is a constant gain matrix. When K and all the associated bounds for the time-varying elements are known, and the perturbation vector $w(t)$ is removed from Eq. (4), we can always write:

$$\dot{x} = \bar{A}x + \sum_{j=1}^{N}[h_j(t)E_j]x \qquad (5)$$

where $\bar{A} = A - BK$ is Hurwitz, $E_j \in \Re^{n\times n}$ is known, and $h_j(t) \in \Re$ is a time-varying function with known strict upper bound $h_{uj} > h_j$ and strict lower bound $h_{lj} < h_j$. We say that such K is "feasible". In this paper, a feasible K is a stabilizing solution if it guarantees uniform global exponential stability of the equilibrium point at the origin of Eq. (5).

To obtain a stabilizing solution for K, we use a 3D graph. Domain of the graph is a two dimensional space of two controller design parameters, namely ρ and η. We use these two parameters to obtain K, and then the corresponding symmetric matrix $Z \in \Re^{n\times n}$. The matrix Z is obtained from the following Theorem 1, which is an extension for multiple input cases of that in [11]. The eigenvalues of Z, denoted by $\lambda(Z)$, are all real. The 3D graph is obtained by plotting the two parameters against the maximum real eigenvalue of Z. A stabilizing solution for K is found at point (ρ^*, η^*) when $\max(\lambda(Z(\rho^*, \eta^*))) < 0$.

Theorem 1 If the dynamical system in Eq. (5) is uniformly globally Lipschitz with $\bar{A}$ being Hurwitz and $\max(\lambda(Z)) < 0$, then the equilibrium point at the origin is uniformly globally exponentially stable. The matrix $Z = Z^T \in \Re^{n\times n}$ is obtained by:

1) Specified Q > 0 and $\bar{A}$ to compute P from the Lyapunov equation $-Q = (1/2)[P\bar{A} + \bar{A}^T P]$

2) Compute $\bar{A}_l = \bar{A} + \sum_{j=1}^{N} h_{lj}E_j$ and $\Phi = P\bar{A}_l + \bar{A}_l^T P$.

3) Compute $\forall j$: $\Psi_j = [PE_j + E_j^T P] = \Psi_j^T$.

4) Compute $\forall j$:

$$\Lambda_{\Psi_j} = T_{\Psi_j}^T \Psi_j T_{\Psi_j} = \mathrm{diag}[\lambda_{\Psi_j 1} \ \dots \ \lambda_{\Psi_j n}].$$

where $T_{\Psi_j} = [v_{\Psi_j 1} \mid \dots \mid v_{\Psi_j n}]$, $\{v_{\Psi_j 1}, ..., v_{\Psi_j n}\}$ is the set of n orthogonal unit (orthonormal) eigenvectors of Ψ_j, and $\{\lambda_{\Psi_j 1}, ..., \lambda_{\Psi_j n}\}$ is the corresponding set of n real eigenvalues of Ψ_j .

5) Set all negative elements of Λ_{Ψ_j} to zero to get $\Lambda_{\Psi_j}^{\geq 0}$ $\forall j$.

6) Compute $\forall j$, $\Psi_j^{\geq 0} = T_{\Psi_j}\Lambda_{\Psi_j}^{\geq 0}T_{\Psi_j}^T$.

7) Compute $Z \equiv \Phi + \sum_{j=1}^{r}[(h_{uj} - h_{lj})\Psi_j^{\geq 0}]$.

Proof We consider the quadratic Lyapunov function $V(x) = (1/2)x^T Px$ in which $P = P^T > 0$. Now, put the matrix $Q = Q^T > 0$ into the Lyapunov equation $-Q = (1/2)[P\bar{A} + \bar{A}^T P]$, and solve for P. Because $\bar{A}$ is Hurwitz, the existence of P, such that all the eigenvalues of P are positive real, is guaranteed [9]. We assert that V(x) is positive definite, decresent, and radially unbounded. It has the following property I:

$$\left(\frac{1}{2}\right)\min(\lambda(P))\|x\|^2 \leq V(x) \leq \left(\frac{1}{2}\right)\max(\lambda(P))\|x\|^2$$

We write for $h_j(t)$, j = 1, 2, ..., N that $h_j(t) = h_{lj} + h_j(t) - h_{lj} = h_{lj} + l_j(t)$, where $l_j(t) = h_j(t) - h_{lj}$. Since $h_{lj} < h_j(t) < h_{uj}$, it follows that $0 < l_j(t) < h_{uj} - h_{lj}$ $\forall j$. Now, substituting $h_{lj} + l_j(t)$ for $h_j(t)$ in Eq. (5) yields:

$$\dot{x} = \bar{A}_l x + \sum_{j=1}^{N} l_j(t)E_j x$$

where $\bar{A}_1$ is defined previously.

Because V(x) does not depend explicitly on t, the time derivative of V(x) along trajectory of the above equation is given by $\dot{V}(x,t)=(\partial V/\partial x)\dot{x}$. This can be arranged in the following form:

$$\dot{V}(x,t)=\left(\frac{1}{2}\right)x^T\Phi x+\left(\frac{1}{2}\right)\sum_{j=1}^{N}l_j(t)x^T\Psi_j x$$

where Φ and Ψ_j are defined previously. Since $\Psi_j^T=\Psi_j\ \forall j$, Ψ_j has a set of n real eigenvalues $\{\lambda_{\Psi_j 1},\ \dots\ ,\lambda_{\Psi_j n}\}$ and the corresponding set of n orthonormal eigenvectors $\{v_{\Psi_j 1},\ \dots\ ,v_{\Psi_j n}\}$. Using the linear transformation $x=T_{\Psi_j}z$, we now write $x^T\Psi_j x=z^T[T_{\Psi_j}^T\Psi_j T_{\Psi_j}]z\equiv z^T\Lambda_{\Psi_j}z$ where T_{Ψ_j} and Λ_{Ψ_j} are defined previously. Then set all negative elements of $\Lambda_{\Psi j}$ to zeros to obtain $\Lambda_{\Psi j}^{\ge 0}$. Because $z^T[\Lambda_{\Psi_j}^{\ge 0}]z\ge 0$, it follows that $z^T[\Lambda_{\Psi j}^{\ge 0}]z\ge z^T\Lambda_{\Psi j}z=x^T\Psi_j x$. Accordingly, we have:

$$z^T[\Lambda_{\Psi_j}^{\ge 0}]z=x^T[T_{\Psi_j}^{-1}]^T[\Lambda_{\Psi_j}^{\ge 0}][T_{\Psi_j}^{-1}]x=x^T\Psi_j^{\ge 0}x$$

where $\Psi_j^{\ge 0}=[T_{\Psi_j}^{-1}]^T[\Lambda_{\Psi_j}^{\ge 0}][T_{\Psi_j}^{-1}]$. Because the matrix T_{Ψ_j} is orthogonal, $T_{\Psi_j}^{-1}=T_{\Psi_j}^T$ and $\Psi_j^{\ge 0}=[T_{\Psi_j}][\Lambda_{\Psi_j}^{\ge 0}][T_{\Psi_j}^T]$. Because $[\Psi_j^{\ge 0}]^T$ $=\Psi_j^{\ge 0}$ and $(h_{uj}-h_{lj})>l_j(x)>0$, it follows that $l_j(t)[x^T\Psi_j x]\le(h_{uj}-h_{lj})[x^T\Psi_j^{\ge 0}x]\ \forall x$ and $\forall t$. This inequality implies that:

$$\dot{V}(x,t)\le\frac{1}{2}x^T\Phi x+\frac{1}{2}\sum_{j=1}^{r}((h_{uj}-h_{lj})[x^T\Psi_j^{\ge 0}x])$$

By letting $Z\equiv\Phi+\sum_{j=1}^{r}[(h_{uj}-h_{lj})\Psi_j^{\ge 0}]$, we have shown that $\dot{V}(x,t)\le(1/2)x^TZx$. If $\max(\lambda(Z))<0$, then the following property II is true $\forall x$ and $\forall t$:

$$\dot{V}(x,t)\le-\left(\frac{1}{2}\right)|\max(\lambda(Z))|\|x\|^2$$

Because V(x) is positive definite, decresent, and radially unbounded, Properties I and II indicate that the equilibrium point at the origin of Eq. (5) is uniformly globally exponentially stable [9]. This completes the proof.

In practical applications of a SCARA, we expect the existence of the perturbation vector w(t) that has been removed previously to facilitate derivation of Theorem 1. With this, we do not expect all trajectories to converge uniformly and exponentially to the origin. Rather, it is reasonable that they converge into a neighborhood about the origin, and the size of this neighborhood depends on the magnitude of perturbation. This is a type of stability known as input-to-state stability [9]. It turns out that this is our case as shown in Corollary 1:

Corollary 1 If Theorem 1 is satisfied, then the origin of the system in Eq. (4) is input-to-state stable.

Proof Following the proof of Theorem 1, we have along the trajectory of Eq. (4) that

$$\dot{V}(x,t)=\left(\frac{1}{2}\right)x^T\Phi x+\left(\frac{1}{2}\right)\sum_{j=1}^{N}l_j(t)x^T\Psi_j x+\left(\frac{\partial V}{\partial x}\right)w(t)$$

Then, $\dot{V}(x,t)\le(1/2)x^TZx+(\partial V/\partial x)w(t)$. Now, we let $w(t)$ be strictly bounded by $\phi\in\Re^+$ and notice that $\partial V/\partial x=x^TP$. Thus,

$$\dot{V}(x,t)\le\left(\frac{1}{2}\right)x^TZx+\max(\lambda(P))\phi\|x\|$$

where $\max(\lambda(P))>0$ because $P=P^T>0$. If we have that $\max(\lambda(Z))<0$, then:

$$\dot{V}(x,t)\le-\left(\frac{1}{2}\right)|\max(\lambda(Z))|\|x\|^2+\max(\lambda(P))\phi\|x\|$$

For any given bound ϕ on $w(t)$, this implies the existence of the corresponding region $\Omega\in\Re^n$ in which x is radially sufficiently large such that $\dot{V}(x,t)<0$ in $\Omega\ \forall t$. Because

V(x) is positive definite, decresent, and radially unbounded, this implies that all the trajectories converge to the region $\Re^n - \Omega$ about the origin from all initial conditions in $\Omega \; \forall t$. Input-to-state stability is asserted, and the proof is completed.

We now give a compact procedure for generating K from two controller design parameters ρ and η, and the 3D plot of $\max(\lambda(Z))$ versus these parameters. The resulting K is guaranteed to be feasible, and is special in that it is a good candidate for forcing $\dot{V}(x,t)$ to be negative definite without relying on the exact expression of $h_j(t)$ [11]. The procedure may be concluded in the followings:

1) Define a two dimensional domain of $\rho > 0$ and $\eta \geq 1$, and select a grid size for this domain. For each coordinate of (ρ, η), execute the following steps 2) – 5)

2) Solve for P from

$$-2I = PA + A^TP - 2\rho PBB^TP$$

The existence of a unique positive definite symmetric solution P is guaranteed.

3) Compute $K = \eta\rho B^TP$, $\bar{A} \equiv A - BK$, and then $Q = -(1/2)[P\bar{A} + \bar{A}^TP]$. The matrix $\bar{A}$ is guaranteed to be Hurwitz.

4) Use ($\bar{A}$, Q) obtained in step 3) to compute Z by executing steps 2) – 7) in Theorem 1.

5) Plot $\max(\lambda(Z))$ versus ρ and η.

Generating this 3D graph of $\max(\lambda(Z))$ versus ρ and η can be automated in a PC relatively easily. Using MATLAB, the maximum processing time for all cases we investigated was less than 5 seconds on a PC with a Pentium D CPU.

4. A Numerical Example

Numerical simulations of SCARAs

Numerical simulations of SCARAs operating in various situations with different sets of robot parameters can be founded in the literature. Here, we examine the simulation example in [7] because it describes a practical situation with sufficient details for us to do comparable simulations. In addition, the associated robot parameters are reasonable in our opinion. These are m_1 = 2.61 kg, m_2 = 3.45 kg, L_1 = 0.3 m, L_{c1} = 0.178 m, L_{c2} = 0.2 m, I_1 = 0.198 kg.m^2, and I_2 = 0.184 kg.m^2. Although not included in [7], we add to this manipulator at the tip of link 2 as in Fig. 1 a loading object of time-varying mass:

$$m_p(t) = 0.3m_2(\sin(t) + 1) \leq 0.6m_2$$

The corresponding object shaping parameter is set to $c_p = 0.005$, which could be interpreted as a cylinder of radius $r_p = 0.1$ m.

From the above data, the relevant matrices in Eq. (4) are given by:

$$A = \left[\begin{array}{c|cc} 0_{4\times2} & \multicolumn{2}{c}{I_{4\times4}} \\ \hline 0_{2\times2} & 0_{2\times1} & A^*_{2\times3} \end{array}\right], \quad B = \left[\begin{array}{c} 0_{4\times2} \\ \hline B^*_{2\times2} \end{array}\right]$$

$$\Delta A = \left[\begin{array}{c|cc} 0_{4\times2} & \multicolumn{2}{c}{I_{4\times4}} \\ \hline 0_{2\times2} & 0_{2\times1} & \Delta A^*_{2\times3} \end{array}\right], \quad \Delta B = \left[\begin{array}{c} 0_{4\times2} \\ \hline \Delta B^*_{2\times2} \end{array}\right]$$

where the constant matrices are

$$A^* = \begin{bmatrix} -0.30 & -0.28 & -0.42 \\ -2.56 & -4.26 & -2.49 \end{bmatrix},$$

$$B^* = \begin{bmatrix} -2.18 & 1.74 \\ 1.74 & -8.98 \end{bmatrix},$$

and the time-varying matrices are ΔA^* and ΔB^*. For all the ten (i, j) time-varying elements of these matrices, all the associated lower bounds h_l are zero while the upper bounds h_u are given in Tables.1 - 2. Notice that some uncertainty bounds are significantly larger than their corresponding nominal values.

Using the above modeling specifications, we follow the procedure given in Section 3 to plot a 3D graph of max $\lambda(Z(\rho,\eta))$ versus ρ and η as in Figure 2. The figure shows that there are infinitely many coordinates (ρ,η) for which max $\lambda(Z(\rho,\eta)) < 0$. We simply select that coordinate $(\rho^*, \eta^*) = (3, 90)$, which yields $\max(\lambda(Z(\rho^*, \eta^*))) = -0.04$. Our investigation strongly suggests that other coordinates of these two controller design parameters could yield better tracking performance but we do not pursue them because this can demonstrate our controller design procedure already.

Table1. Upper bounds on the (i, j) elements of ΔA^* (lower bounds are all zero).

(i, j)	(1, 1)	(1, 2)	(1, 3)	(2, 1)	(2, 2)	(2, 3)
h_u	1.75	2.38	2.00	3.18	4.70	3.23

Table2. Upper bounds on the (i, j) elements of ΔB^* (lower bounds are all zero).

(i, j)	(1, 1)	(1, 2)	(2, 1)	(2, 2)
h_u	0.97	1.92	1.92	5.08

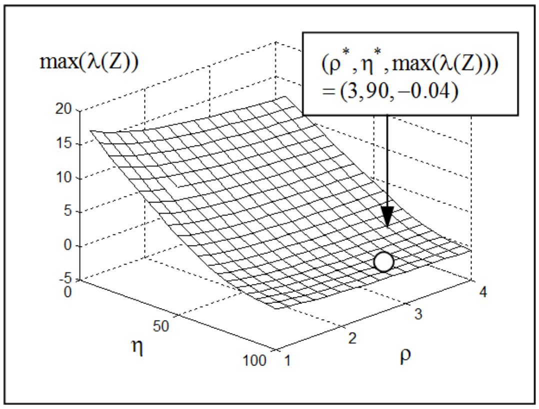

Figure 2. A 3D graph of $\max \lambda(Z(\rho, \eta))$ versus design parameters ρ and η, with the selected pair $(\rho^*, \eta^*) = (3, 90)$ marked by a sphere.

The corresponding feedback gain matrix K is now obtained as:

$$K = \begin{bmatrix} -156 & -10.9 & -294 & -5.5 & -173 & 2.4 \\ 10.9 & -156 & 14.9 & -260 & 28 & -150 \end{bmatrix}$$

We substitute the control torque vector $T_c = -Kx$ and the disturbing torque vector T_d in the nonlinear model of Eq. (1), and run numerical simulations. From [7], the joint reference trajectories are $r_1(t) = \sin(t)$, and $r_2(t) = \cos(t)$, with joint initial conditions $q_1(0) = 1.5$ rad, $q_2(0) = -1.5$ rad, and $\dot{q}_1(0) = \dot{q}_2(0) = 0$ rad/s. Both joints are subjected to square-wave external disturbing torques T_{d1} and T_{d2} of magnitude ±5 N.m and period $\pi/5$ s. Our simulation results are given in Figure 3, while those from [7] are provided in Figure 4-5 for convenience of the readers.

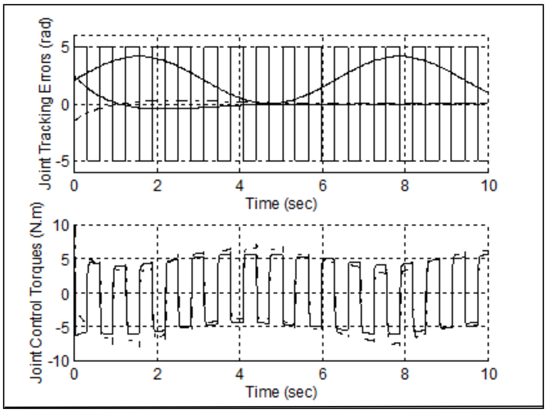

Figure 3. (Upper) Joint tracking errors $e_1(t) = x_3(t)$ (dash-dot: rad), $e_2(t) = x_4(t)$ (solid: rad), disturbing torque T_{d1} and T_{d2} (sq. wave: N.m), and time-varying mass $m_p(t)$ (sinusoidal: ×2 kg) (Lower) Control torque T_{c1} (dash-dot: N.m), and T_{c2} (solid: N.m).

We note that the signs of the joint tracking errors and the corresponding control torques in ours are the opposite of those in [7] by definitions. Because our case is associated with the time-varying mass $m_p(t)$ at the tip of link 2, while [7] is not, comparisons should be made carefully. When compared to the simulation results in [7], our joint tracking errors have smaller rise time but with larger overshoot. From both papers, convergence of the trajectories into small neighborhoods about the origin is obvious, and various characteristics of the control torques are similar. After a transient period of 6 seconds, our joint errors and control torques are bounded by ±0.02 rad and ±7.5 N.m respectively. The latter set of data is not given explicitly in [7], but one could estimate it roughly from the simulations provided in Figure 4-5. All the simulations indicate that both techniques could yield very satisfactory tracking performance.

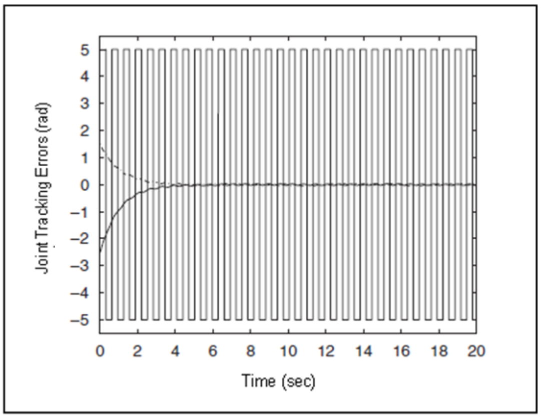

Figure 4. Joint tracking errors $e_1(t)$ (dash-dot: rad), $e_2(t)$ (solid: rad), and disturbing torque T_{d1} and T_{d2} (sq. wave: N.m), with $m_p(t) = 0$ [7].

Recall that the above simulations are associated with large initial conditions of $e_1 = -1.5$ rad, $e_2 = 2.5$ rad, $\dot{e}_1 = 1$ rad/s, and $\dot{e}_2 = 0$ rad/s. The corresponding magnitude of the control torques in ours and [7] are then large during an initially short period of time. This does not occur in practical operation, in which the robot is set to start at small values of $e_i(0)$ and $\dot{e}_i(0)$ to avoid amplifier saturation and unnecessary stress to the robot.

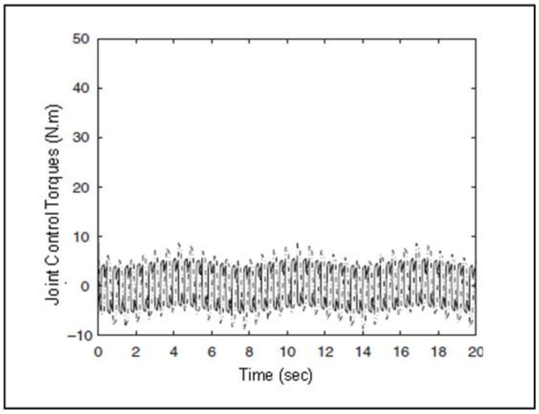

Figure 5. Control torque T_{c1} (dash-dot: N.m), and T_{c2} (solid: N.m), with $m_p(t) = 0$ [7].

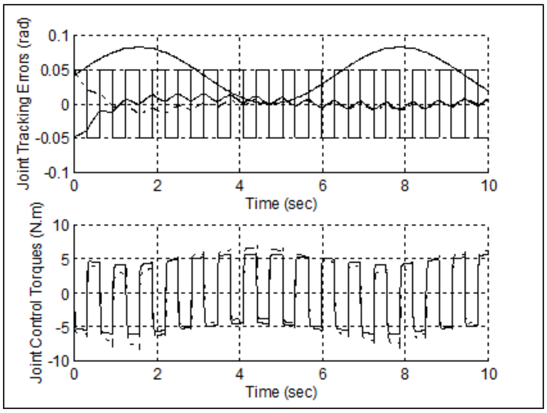

Figure 6. (Upper) Joint tracking errors $e_1(t) = x_3(t)$ (dash-dot: rad), $e_2(t) = x_4(t)$ (solid: rad), disturbing torque T_{d1} and T_{d2} (sq. wave: $\times 0.01$ N.m), and time-varying mass $m_p(t)$ (sinusoidal: $\times 0.04$ kg) (Lower) Control torque T_{c1} (dash-dot: N.m), and T_{c2} (solid: N.m).

To examine such a practical case, we set $e_1 = 0.05$ rad, $e_2 = 0.05$ rad, and $\dot{e}_1 = \dot{e}_2 = 0$ rad/s. In this case, our simulations reveal that the initial control torques are bounded by ± 14.5 N.m. Then they decreases very quickly to stay within ± 7.5 N.m as shown in Figure 6. Tracking errors are bounded by ± 0.02 rad after 6 seconds as in the previous case. The bounds on the control torques are quite reasonable, given that the joints are subjected to external disturbing torques T_{di} of ±5 N.m. When the upper bound of $m_p(t)$ reduces, our additional simulations (not shown here) indicate that the bounds on control torques reduce accordingly.

5. Conclusion

This paper presents an innovative graphical technique for designing a linear PID controller with applications to trajectory tracking of SCARAs. In the beginning, we propose the use of a linear model that fully accounts for time-varying elements in the system matrix and the input matrix that appear when linearizing the robot nonlinear model about the equilibrium point at the origin. This effectively extends the region in state space for which our model can closely approximate the original dynamics of the robot of interest. We use the Lyapunov stability theorem to develop Theorem 1 and Corollary 1. Together, they constitute a criterion for determining convergence of all trajectories belonging to our model into a neighborhood about the origin, with an estimate for the size of this neighborhood included. We use this criterion to plot a 3D graph whose domain is a space of two real controller design parameters. This graph yields a stabilizing controller when the range of the graph, which is always real, is negative at some point.

Our PID controller for SCARA trajectory tracking is theoretically justified, is relatively simple to obtain, and is easy to implement. These nice characteristics thus allow its applications in a large variety of situations. When considering tracking performance, it appears from the literature that ours is very satisfactory. In addition, our linear control law always guarantees the desirable property of smoothness for control inputs, especially when compared to those obtained by incorporating switching schemes. It is then reasonable to expect that our controller neither excites hidden dynamics of the robots, nor causes undesirable heat due to finite switching time of robot amplifiers. Now, we are investigating additional useful features and areas of potential applications associated with our graphical approach. In particular, we are determining if a useful concept of relative stability could be introduced for linear systems subjected to nonlinear time-varying uncertainties in a practical manner. We are also examining the situation in which our approach could be preferable to a numerical optimization approach such as LMI (Linear Matrix Inequality).

6. References

[1] A. Visioli, and G. Legnani, On the Trajectory Tracking Control of Industrial SCARA Robot Manipulators, IEEE Trans. on Industrial Electronics, Vol. 49, No.1, pp. 224-232, February 2002.

[2] S. Suvilath, et. al., IMC Based PID Controllers Design for a Two-Links SCARA Robot, IEEE TENCON 2011, pp. 1030-1034, 2011.

[3] T. C. S. Hsia et. al., Robust Independent Joint Controller Design for Industrial Robot Manipulators, IEEE Transactions on Industrial Electronics, Vol. 38, No.1, pp. 21-25, February 1991.

[4] P. Khosla, and T. Kanade, Real-Time Implementation and Evaluation of Computed-Torque Scheme, CMU-RI-TR-87-6, Carnegie Mellon University, 1987.

[5] L. C. Fu, and T. L. Liao, Globally Stable Robust Tracking of Nonlinear Systems Using Variable Structure Control with an Application to a Robotics Manipulator, IEEE Transaction on Automatic Control, Vol. 35, pp. 1345-1350, 1990.

[6] N. Nersisian, and R. Zanasi, A Modified Variable Structure Control Algorithm for Stabilization of Uncertain Dynamical Systems, Int. J. of Robust Nonlinear Control, Vol. 3, pp. 199-209, 1993.

[7] C.-S. Tseng, Robust Tracking Control Design for Uncertain Robotic Systems with Persistent Bounded Disturbances, Asian Journal of Control, Vol. 10, No. 4, pp.420-429, July 2008.

[8] G. Hasannifard et. al., Robust Nonlinear Control of Two Links Robot Manipulator and Computing Maximum Load, World Academy of Science, Engineering and Technology, Vol. 3, pp. 927-932, 2009.

[9] H. K. Khalil, Nonlinear Systems, 3rd Edition, Prentice Hall, New Jersey, 2000.

[10] J.-J Slotine, and W. Li, Applied Nonlinear Control, Prentice-Hall, 1991.

[11] P. Ngamsom, and L. L. Hoberock, Using Robust Stability Analysis Theorems for Robust Controller Design, ASME Journal Of Dynamic Systems, Measurement, and Control, Vol. 125, No. 4, pp. 669-671, 2003.

[12] C. J. Fallaha, M. Saad, H.Y. Kanaan, and K. Al-Haddad, Sliding-Mode Robot Control with Exponential Reaching Law, IEEE Transactions on Industrial Electronics, Vol. 58, No. 2, pp. 600-610, 2011.

[13] S. Islam, and P.X. Liu, Robust Sliding Mode Control for Robot Manipulators, IEEE Transactions on Industrial Electronics, Vol. 58, No. 6, pp. 2444-2453, 2011.